FEMS Microbiology Ecology, 94, 2018, fiy171

doi: 10.1093/femsec/fiy171
Advance Access Publication Date: 0 2018
Research Article

RESEARCH ARTICLE

Steep redox gradient and biogeochemical cycling driven by deeply sourced fluids and gases in a terrestrial mud volcano

Yueh-Ting Lin[1,†], Tzu-Hsuan Tu[1,2,†], Chih-Lin Wei[2], Douglas Rumble[3], Li-Hung Lin[1] and Pei-Ling Wang[2,*]

[1]Department of Geosciences, National Taiwan University, 1 Sec 4 Roosevelt Rd., Taipei 10617, Taiwan, [2]Institute of Oceanography, National Taiwan University, 1 Sec 4 Roosevelt Rd., Taipei 10617, Taiwan and [3]Geophysical Laboratory, Carnegie Institute of Washington, 5251 Broad Branch Rd., NW Washington DC 20015, USA

*Corresponding author: Institute of Oceanography, National Taiwan University, 1 Sec 4 Roosevelt Rd., Taipei 10617, Taiwan. Tel: +886 233661390; E-mail: plwang@ntu.edu.tw

One sentence summary: In this study, deep subsurface-sourced fluids are seeded with microorganisms at shallow depths and producing a steep redox gradient that shapes the metabolic zonation in a methane-rich mud volcano ecosystem.

Editor: Matthew Stott

†Equal contribution.

ABSTRACT

Mud volcanoes provide an accessible channel through which deep subsurface environments can be observed. The manner in which deeply sourced materials shape biogeochemical processes and microbial communities in such geological features remains largely unknown. This study characterized redox transitions, biogeochemical fluxes and microbial communities for samples collected from a methane-rich mud volcano in southwestern Taiwan. Our results indicated that oxygen penetration was confined within the upper 4 mm of fluids/muds and counteracted by the oxidation of pyrite, dissolved sulfide, methane and organic matter at various degrees. Beneath the oxic zone, anaerobic sulfur oxidation, sulfate reduction, anaerobic methanotrophy and methanogenesis were compartmentalized into different depths in the pool periphery, forming a metabolic network that efficiently cycles methane and sulfur. Community members affiliated with various Proteobacteria capable of aerobic oxidation of sulfur, methane and methyl compounds were more abundant in the anoxic zone with diminished sulfate and high methane. These findings suggest either the requirement of alternative electron acceptors or a persistent population that once flourished in the oxic zone. Overall, this study demonstrates the distribution pattern for a suite of oxidative and reductive metabolic reactions along a steep redox gradient imposed by deep fluids in a mud volcano ecosystem.

Keywords: microelectrode; sulfur; methane; microbial seedbank; mud volcano; Taiwan

INTRODUCTION

Deep subsurface environments have been estimated to harbor up to 5 × 10^{30} cells, probably with equal contributions from the terrestrial and marine realms (Onstott *et al.* 1998; Whitman, Coleman and Wiebe 1998; Lipp *et al.* 2008; Kallmeyer *et al.* 2012; McMahon and Parnell 2014). Such a huge quantity of biomass constitutes the largest microbial reservoir on Earth, and

Received: 12 March 2018; **Accepted:** 24 August 2018

can profoundly affect the cycling of carbon, nitrogen and sulfur between the crust, hydrosphere, and atmosphere on contemporary and geological time scales (Whitman, Coleman and Wiebe 1998). However, uncovering the distribution, diversity, composition and function of microbial communities inhabiting deep subsurface environments is challenging, owing to rare and costly access to representative samples.

Mud volcanoes (MVs) are cone shaped, circular manifestations on land or the seafloor, and represent the expression of a fracture network that often extends to a depth of several kilometers (Mazzini and Etiope 2017). As advection dominates over diffusion for fluid transport in a fracture network, relatively rapid migration can occur with minimal alterations of the fluid and gas emanating from a mud cone or pool (Dimitrov 2002). Therefore, MVs provide a direct, effective means to recover deep microbial communities and fluid characteristics, and constrain the connectivity of a deep source to shallow groundwater. In addition, deeply seated communities could have been impacted by a number of environmental factors since their initial deposition on the seafloor (Starnawski *et al.* 2017). The manner in which microbial communities respond to such changes over the course of various geological processes (e.g. compaction, pressure-temperature change and fault displacement) remains largely unknown.

Despite the continuous delivery of deeply sourced materials into surface environments, the physical and chemical contexts of MVs are greatly controlled by the dynamic interplay between biotic and abiotic processes (Mazzini and Etiope 2017). Among these processes, the most striking appears to be the penetration of atmospheric oxygen, through which the reducing power associated with the upward transport fluids is counteracted (Boetius and Wenzhöfer 2013). The oxidant-reductant interaction produces a redox gradient that leads to the proliferation and coexistence of microorganisms with a spectrum of oxygen affinity and metabolic capability (Nisbet and Sleep 2001), and facilitates the regeneration of electron acceptors, and energy and material exchange at the oxic–anoxic boundary (Thomson *et al.* 1993). Previous studies using a static chamber or microelectrode have shown that a significant fraction of total/diffusive oxygen fluxes or oxygen uptake rates in marine seeps or MVs (mostly >50%) are accounted for by aerobic methane oxidation near the seafloor (Boetius and Wenzhöfer 2013; Khripounoff *et al.* 2015). Thiotrophic and organotrophic oxygen consumption plays a relatively minor role, even though sulfate is abundant. Whether the pattern and magnitude of oxygen penetration and dominant metabolism responsible for oxygen consumption in marine settings could be directly extrapolated to terrestrial counterparts with an infinitely large oxygen reservoir and scarce sulfate is not well established.

This study aims to determine the biogeochemical processes and element cycling imposed by the discharge of deeply sourced, reducing materials in the Shin-Yan-Ny-Hu (SYNH) MV of southwestern Taiwan. Vertical concentration profiles of dissolved oxygen and sulfide at millimeter resolution, and of sulfate, methane and dissolved inorganic carbon (DIC) at centimeter resolution were obtained for samples distributed in different compartments of the MV. These data were integrated with the abundance of specific taxonomic groups based on the 16S rRNA gene, alpha subunit of particulate methane monooxygenase gene (*pmoA*), and beta subunit of dissimilatory sulfite reductase gene (*dsrB*) to constrain the material fluxes, and determine the origins of microbial communities, and niche and metabolic compartmentalization along the redox transition in the methane-rich MV ecosystem. Furthermore, the sequence data were compared with those for sediments in the South China Sea to address the dispersal of microbial seedbanks undergoing long-term geological perturbation.

MATERIALS AND METHODS

Site background and field sampling

The SYNHMV is one of the MVs distributed along the NE-SW trending Chishan fault zone in southwestern Taiwan. This fault is part of a series of west-propagating thrust systems formed by the subduction of the Eurasian Plate underneath the Philippine Sea Plate, and is responsible for the exhumation of sediments that had once been deposited in the continental margin and South China Sea (Teng and Lin 2004). The field site is characterized by two circular structures (a cone-shaped mud pie (SYNH01) and a mud pool (SYNH02)). Additional site background is provided in the supplementary methods.

The SYNH02 was selected as our primary field site because vigorous bubbling and fluid discharge created a strong redox gradient and deposited a layer of soft mud in the pool periphery. Before sample collection, several parameters (including temperature, conductivity, pH, redox potential and salinity) of fluids near the main bubbling feature were measured on site using portable probes (Hanna Instruments, Woonsocket, RI, USA). Sampling was performed at stations categorized into three types: (i) bubbling fluids in the pool (names starting with BF), (ii) fluidized muds near the pool margin (names starting with PM) and (iii) muds in the pool periphery (names starting with PP) (Fig. S1, Supporting Information). Field campaigns were conducted in November 2016, June 2017 and August 2017. In brief, bubbling fluids were scooped using a sterilized cup. Fluid and sediment columns in all categories of stations were collected using sterilized core liners. The lengths of the fluid and mud columns were 20 cm and between 10 and 52 cm, respectively.

Simultaneous profiling of dissolved oxygen, pH and hydrogen sulfide was carried out using microelectrodes controlled by a field motor connected to a multimeter (Unisense, Aarhus, Denmark). The tips of the microelectrodes were aligned perpendicular to the surface of fluids/muds. Measurements were carried out at 1-mm resolution until 10–12 cm was reached. Calibrations of microelectrodes for O_2 (OX-100, Unisense, Aarhus, Denmark), hydrogen sulfide (H_2S-100, Unisense, Aarhus, Denmark) and pH (pH-100, Unisense, Aarhus, Denmark) were performed either on site or one day before profiling, in accordance with the manufacturer's recommendation. Detailed calibrations for microelectrode measurements are described in the supplementary methods.

Geochemical analyzes

Detailed sample processing and preservation procedures are described in the supplementary methods. Concentrations of CH_4 and DIC were analyzed using a 6890N gas chromatograph (GC; Agilent Technologies, Santa Clara, CA, USA) equipped with a Porapak Q packed column (3 m), a flame ionization detector and a thermal conductivity detector. Carbon isotope compositions of CH_4 and DIC were measured using a MAT253 isotope ratio mass spectrometer (IRMS) connected with a GC Isolink (Thermo Fisher Scientific, Waltham, MA, USA). Detailed methods for GC ramping and sample acidification could be referred to Chang *et al* (2012). Delta notation ($\delta^{13}C = (R_{sample}/R_{standard} - 1) \times 1000‰$, where R is the ratio of ^{13}C to ^{12}C, and the standard is Vienna Pee

Dee Belemnite) was used in reporting the data. The uncertainty for individual measurements was less than 0.2‰.

Two anions in the filtrates, Cl^- and SO_4^{2-}, were analyzed using an ICS-3000 ion chromatograph (Thermo Fisher Scientific, Waltham, MA, USA). The analysis was carried out in duplicate with an uncertainty of <2%. The CRS (chromium reducible sulfur; operationally defined to be equivalent to pyrite) and AVS (acid volatile sulfur; operationally defined to be equivalent to monosulfide minerals) concentrations were measured using the methods described by Canfield *et al.* (1986). The analysis was carried out in duplicate with an uncertainty of <2%.

Calculations of diffusive fluxes

Diffusive flux was calculated using the following equation:

$$\text{Flux} = \text{porosity} \times \text{diffusivity} \times \text{concentration gradient} \quad (1)$$

Porosity was first calculated from the water content, assuming that the average density of minerals constituting muds was 2.5 g cm^{-3}. The porosities obtained within the target depth interval were averaged. The diffusivity of a specific ion or molecule at 25°C and 6 ppt salinity was adopted from Tse and Sandall (1979), Krom and Berner (1980), Iversen and Jørgensen (1993) and Tamimi *et al.* (1994). Maximum fluxes of dissolved oxygen at the air-fluid/mud interface were calculated for all stations. Averaged fluxes of sulfide near the air-fluid/mud interface and/or at depths below the sulfate-depletion zone in the pool periphery were calculated. Averaged fluxes of sulfate were also calculated for stations near the pool margin and in the pool periphery, where downward-decreasing sulfate concentrations were clear. Additional calculations were performed for the air–mud interface considering a concentration gradient between the bubbling fluid and the top pore water, and for the upper few centimeters at stations PP4, PP8 and PP9, where downward-increasing sulfate concentrations were observed. Averaged fluxes of methane were calculated only for stations in the pool periphery.

DNA extraction and 16S rRNA gene analyzes

The DNA was extracted from 2 to 5 g of samples from the bubbling fluids (BF2016 and BF16–2.5 cm), and all samples from stations PP4 and PP11 using the PowerSoil DNA Isolation Kit (Qiagen, Hilden, Germany). The DNA extracts were stored at −80°C for subsequent analyzes.

Polymerase chain reaction (PCR) amplification was applied to the DNA extracts obtained from 11 depths at station PP4, all depths at station PP11 and two bubbling fluids using the primers F515 (5′–GTG CCA GCM GCC GCG GTA A–3′) and R806 (5′–CCC GTC AAT TCM TTT RAG T–3′) for the V4 region of 16S rRNA genes. Although these primers have been reported to be less efficient in generating archaeal amplicons (Parada *et al.* 2016), they were used to facilitate the comparison with other studies. The schemes and reagents for PCR and downstream processing of amplicons were the same as those described in Tu *et al.* (2017).

Quantitative PCR (qPCR) was used to analyze the copy numbers of 16S rRNA genes for bacteria, archaea and ANME-1, and of *dsrB* genes for sulfate reducers and *pmoA* genes for types I and II aerobic methanotrophs in all DNA extracts using a MyiQ Real Time PCR Detection System (Bio-Rad, Hercules, CA, USA). Standard preparations, primers for 16S rRNA genes and PCR conditions were the same as those described in Wang *et al.* (2014) and Tu *et al.* (2017). Primer combinations of DSRp2060F/DSR4R (Geets *et al.* 2006) and A189F/mb661r (Costello and Lidstrom 1999) were used to quantify the abundance of *dsrB* and *pmoA* genes, respectively. The copy numbers of genes were calculated with the length of amplicon, assuming 650 g mol^{-1} of one base pair of DNA.

Sequence analyzes of 16S rRNA gene amplicons

Sequences of 16S rRNA gene amplicons were analyzed using the Mothur 1.35 following the standard protocols described by Schloss *et al.* (2009). Unique reads were aligned to the Silva SSU dataset of the NR 128 release (www.silva.org). Reads not aligned in the same region were removed. Sequence regions beyond the primers were truncated. Potential chimeric sequences were detected and removed using the UCHIME program (Edgar *et al.* 2011). The obtained sequences were deposited in the GenBank with the accession number SRP133776. The number of sequences in each sample after quality filtering is shown in Table S1 (Supporting Information).

Taxonomy of each unique sequence was assigned using the Silva SSU dataset of the NR 128 release as the reference. Taxonomy assignments with bootstrap values greater than 80% were considered valid. Sequences sharing more than 97% identity were further clustered into individual operational taxonomic units (OTUs) using the nearest neighbor algorithm (Schloss and Westcott 2011). Based on the rarefied dataset ($n = 26{,}927$), alpha diversity indices, such as the numbers of observed OTUs, Chao1 and inverse Simpson indices (Hill 1973; Chao, Sederoff and Levings 1984; Faith 1992), were computed. The dissimilarity matrix between samples was computed using the Bray-Curtis method (Bray and Curtis 1957) and visualized through the ordination of non-metric multidimensional scaling (NMDS).

RESULTS

Geochemical characteristics

Fluid temperatures, pH and redox potentials in the main bubbling feature (near station BF16) varied from 42°C to 46°C, 7.75 to 8.29 and −108 to −97 mV, respectively, during three field trips. The temperature decreased rapidly to the ambient level as the distance from the bubbling feature increased (Fig. S1, Supporting Information).

Samples retrieved from near the bubbling features in the pool (stations BF15 to BF19) were characterized by high water content (>50 wt% with most values around 60 wt%; Fig. S2, Supporting Information) and relatively low and uniform chloride (93 to 102 mM) and sulfate (most less than 40 μM) concentrations (Fig. 1). Methane concentrations ranged between 0.8 and 3.3 mM with most $\delta^{13}C$ values being around -34 ± 1‰. One exception occurred at station BF15, where $\delta^{13}C$ values ranged between −42 and −35‰, with the top one being most depleted in ^{13}C. The DIC concentrations ranged between 16 and 24 mM, and generally increased with increasing depth, with most $\delta^{13}C$ values being around -0.7 ± 0.2‰. Dissolved oxygen concentrations decreased sharply from a concentration near the atmospheric equilibrium to one below the detection limit in the upper 4.0 mm (Fig. 1). Sulfide concentrations generally increased with increasing depth. The depth ranges for the abrupt increase from low to high sulfide concentrations (up to ∼180 μM) varied among sites.

Samples retrieved from near the pool margin (stations PM10, PM13 and PM14) were characterized by decreasing water content (50–55 wt% at the top) with increasing depth (Fig. S2, Supporting Information). Chloride and sulfate concentrations ranged

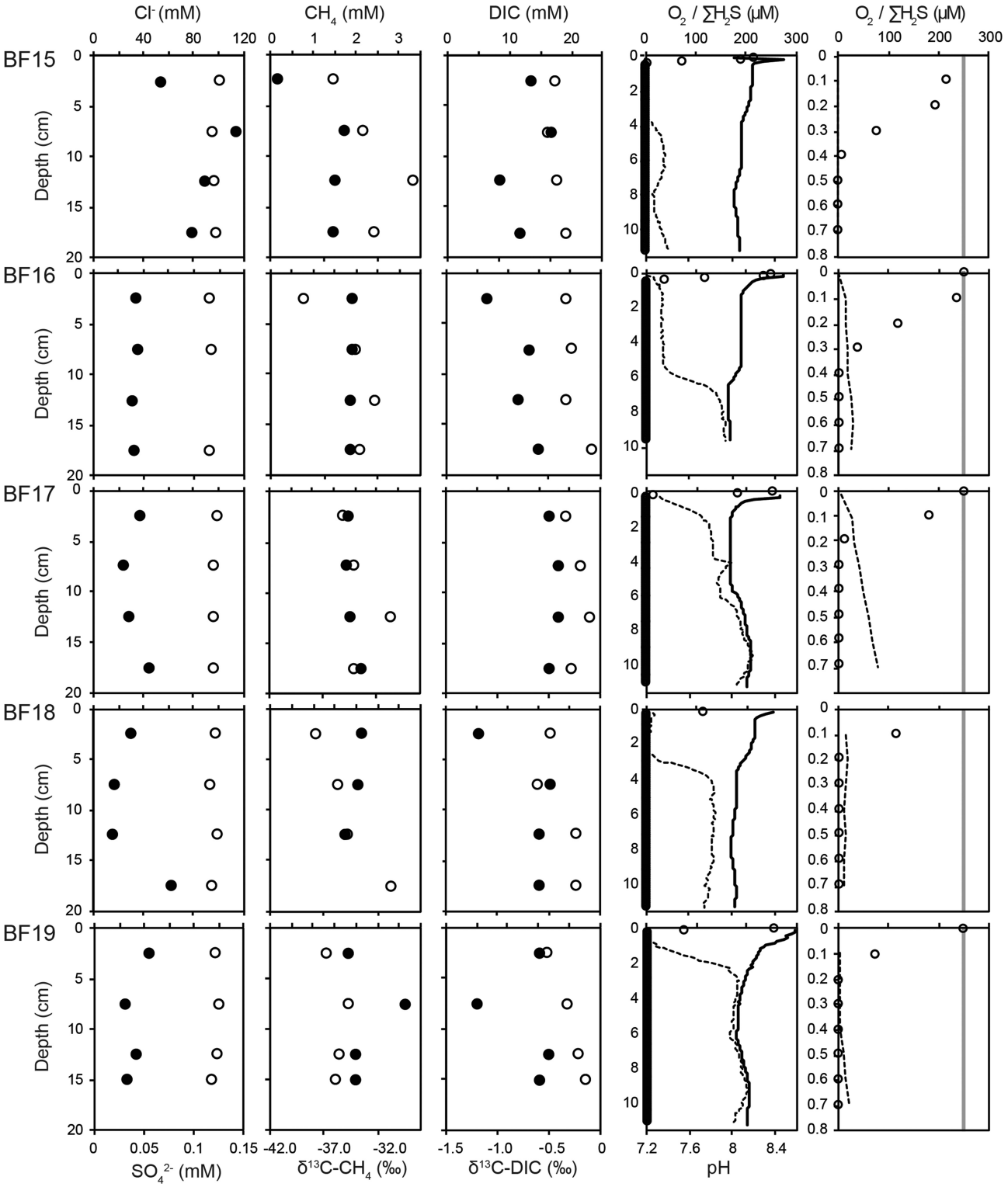

Figure 1. Geochemical profiles for the samples collected from the mud pool (stations BF15-BF19). Open symbols and dashed line represent the concentrations referred to the top axis (chloride, methane, DIC, dissolved oxygen and sulfide), whereas solid symbols represent the concentrations and isotopic compositions referred to the bottom axis (sulfate, $\delta^{13}C$ values of methane and DIC, and pH). The profiles of dissolved sulfide and pH in the upper 0.8 cm were further magnified in the panels to the right for better visualization of the concentration variation near the air-fluid interface. The concentration of dissolved oxygen in equilibrium with the atmospheric oxygen under the *in situ* condition is marked with a gray line at 249.3 μM.

mostly between 86 and 119 mM and between 30 and 170 μM, respectively, with small magnitudes of variations along depths (Fig. 2). Methane concentrations ranged between 0.01 and 2.6 mM and increased with increasing depth. In contrast, $\delta^{13}C$ values of methane decreased with increasing depth. The DIC concentrations ranged between 13 and 22 mM, whereas its $\delta^{13}C$ values varied between −0.3 and 2.9‰. Dissolved oxygen concentrations decreased sharply with increasing depth, and varied in a pattern similar to that observed for the pool fluids. Sulfide concentrations at stations PM10 and PM13 increased from below the detection limit to 120–386 μM at 2 cm, followed by small variations between 2 and 4 cm, and a decreasing trend with increasing depth thereafter.

Samples retrieved from the pool periphery (stations PP4, PP8, PP9, PP11 and PP12) were characterized by 23–52 wt% water content. At stations PP4, PP8 and PP9, water content decreased sharply below 5–10 cm (Fig. S2, Supporting Information). Chloride concentrations (up to 238.7 mM) generally decreased with increasing depth (Fig. 3). Variations in sulfate concentration could have been categorized into two patterns. The first type (stations PP4, PP8 and PP9) was characterized by an increase of up to 1.7 mM in the upper 10–20 cm, followed by a sharp decline to below the detection limit further down. The other type of pattern was characterized by a decreasing trend with increasing depth. Whereas methane concentrations increased from tens of micromolar to up to 4.0 mM with increasing depth, its $\delta^{13}C$ values decreased from around –35‰ to as low as –53‰ with increasing depth. The DIC concentrations and isotopic compositions exhibited various depth-dependent patterns. Dissolved oxygen concentrations decreased sharply to below the detection limit in the upper 2 mm. Sulfide concentrations increased to up to 630 μM with increasing depth at stations PP11 and PP12. Pyrite concentrations ranged between 0.7 and 1.0 mg-S g^{-1} with relatively high values (0.90 ± 0.02 mg-S g^{-1}) corresponding to the upper sulfate-depletion zone (Fig. S3, Supporting Information) and low values (0.81 ± 0.06 mg-S g^{-1}) at greater depths. The AVS concentrations were below the detection limit for all samples.

Diffusive fluxes of dissolved oxygen, sulfide, sulfate and methane

Downward fluxes of dissolved oxygen near the air-fluid/mud interface ranged between 1.82×10^{-2} and 3.06×10^{-2} mol m^{-2} d^{-1}, whereas upward fluxes of sulfide in the upper 1.6 cm ranged between 6.50×10^{-4} and 9.37×10^{-3} mol m^{-2} d^{-1} (Table 1). Upward sulfide fluxes in the anoxic zone ranged between 1.72×10^{-4} and 1.41×10^{-3} mol m^{-2} d^{-1}. Downward fluxes of sulfate ranged between 1.02×10^{-4} and 6.94×10^{-3} mol m^{-2} d^{-1}, with values in the pool periphery being greater than those near the pool margin. Upward sulfate fluxes ranged between 0 and 1.74×10^{-2} mol m^{-2} d^{-1} in the upper 1 cm and between 2.90×10^{-4} and 1.21×10^{-3} mol m^{-2} d^{-1} at depths above the sulfate maximum. Upward fluxes of methane ranged between 2.73×10^{-4} and 3.40×10^{-3} mol m^{-2} d^{-1}.

Community structures and compositions

Analyzes of 16S rRNA genes yielded 1 397 132 sequences. The numbers of observed OTUs were highest at 32.3 cm at station PP4 and 19.0 cm at station PP11, and decreased toward both the top and bottom of the cores (Table S1, Supporting Information). The trends of the Chao1 and inverse Simpson indices resembled the pattern of observed OTUs. At station PP4, community components shifted from the second quadrant for BF2016 to the third quadrants for the depths with greater $\delta^{13}C$ values of methane and high sulfate, to the second quadrant for the depths with depleted sulfate and finally to the first quadrant for the depths with high methane (Fig. S4, Supporting Information). At station PP11, community components shifted from the second quadrant for BF16–2.5 cm to around the negative NMDS2 axis for the depths with depleted sulfate and to around the positive NMDS1 axis for the depths with high methane. Such changes of community compositions were correlated with depth ($R^2 = 0.60$, $P < 0.01$), sulfate ($R^2 = 0.55$, $P < 0.01$), chloride ($R^2 = 0.48$, $P < 0.01$), methane ($R^2 = 0.52$, $P < 0.01$) and $\delta^{13}C$ values of methane ($R^2 = 0.47$, $P < 0.01$).

A total of 25 482 bacterial and 1167 archaeal OTUs, representing 217 classes (184 bacterial and 33 archaeal) within 82 phyla, were recovered. The dominant bacterial and archaeal phyla (and subdivisions of Proteobacteria; >5% of the total reads) included Atribacteria, Bacteroidetes, Chloroflexi, Deltaproteobacteria, Firmicutes, Gammaproteobacteria and Euryarchaeota (Fig. 4). Proportions of individual phyla varied among individual samples and between stations (Fig. 4; Table S2, Supporting Information). For bubbling fluids, the dominant community members (>0.5%) were related to uncultured microorganisms, and to the families/genera Peptococcaceae, Pseudomonadaceae, *Syntrophorhabdus*, *Thermodesulfovibrio*, *Desulfonatronum*, *Methanosaeta*, *Smithella*, *Marinospirillum* and *Thioalkalispira* (Table S2, Supporting Information). These community members either diminished or declined with increasing depth in cored muds. For cored muds, the abundance of Gammaproteobacteria was high (>50%) in the upper 5–10 cm and decreased with increasing depth. In contrast, the abundance of Atribacteria, Chloroflexi, Deltaproteobacteria, Euryarchaeota and Firmicutes either increased with increasing depth or reached high values at middle depths (Fig. S4, Supporting Information). Sequences of the major OTUs (>0.5%) were related to either uncultured microorganisms or to the families/genera Pseudomonadaceae, *Alcanivorax*, Anaerolineaceae, Comamonadaceae, *Deferrisoma*, *Desulfatitalea*, *Desulfurivibrio*, *Desulfurispirillum*, *Desulfonatronum*, Ectothiorhodospiraceae, *Geoalkalibacter*, *Marinobacter*, *Marinospirillum*, *Methylomicrobium*, *Methylonatrum*, Peptococcaceae, Psuedomonadaceae, *Smithella*, *Thioalkalispira* and *Thioalkalimicrobium* (Table S2, Supporting Information). Their abundance exhibited various patterns along depths.

Quantitative analysis of gene copy number

qPCR analysis indicated that bubbling fluids contained low gene copy numbers of all investigated taxonomic groups (Fig. 5). In cored muds, archaeal 16S rRNA gene copy numbers ranged from the limit of detection to 5.3×10^5 copies g^{-1} at station PP4 and 1.2×10^6 copies g^{-1} at station PP11. Their abundance generally increased with increasing depth, showing high values in the high methane zone. The ANME-1 16S rRNA gene copy numbers ranged from the limit of detection to up to 6.3×10^3 copies g^{-1}. Their abundance peaked in the sulfate-methane transition zone (SMTZ) and declined rapidly toward both shallower and deeper levels. Bacterial 16S rRNA gene copy numbers were up to two orders of magnitude more abundant than archaeal 16S rRNA gene copy numbers. Although their abundance generally increased with increasing depth, relatively high values deviating from the increasing trend were also observed. The abundance of *dsrB* genes ranged from the limit of detection to 3.6×10^4 copies g^{-1} at station PP4 and 3.0×10^5 copies g^{-1} at station PP11. The abundance of *pmo*A genes ranged from the limit of detection to

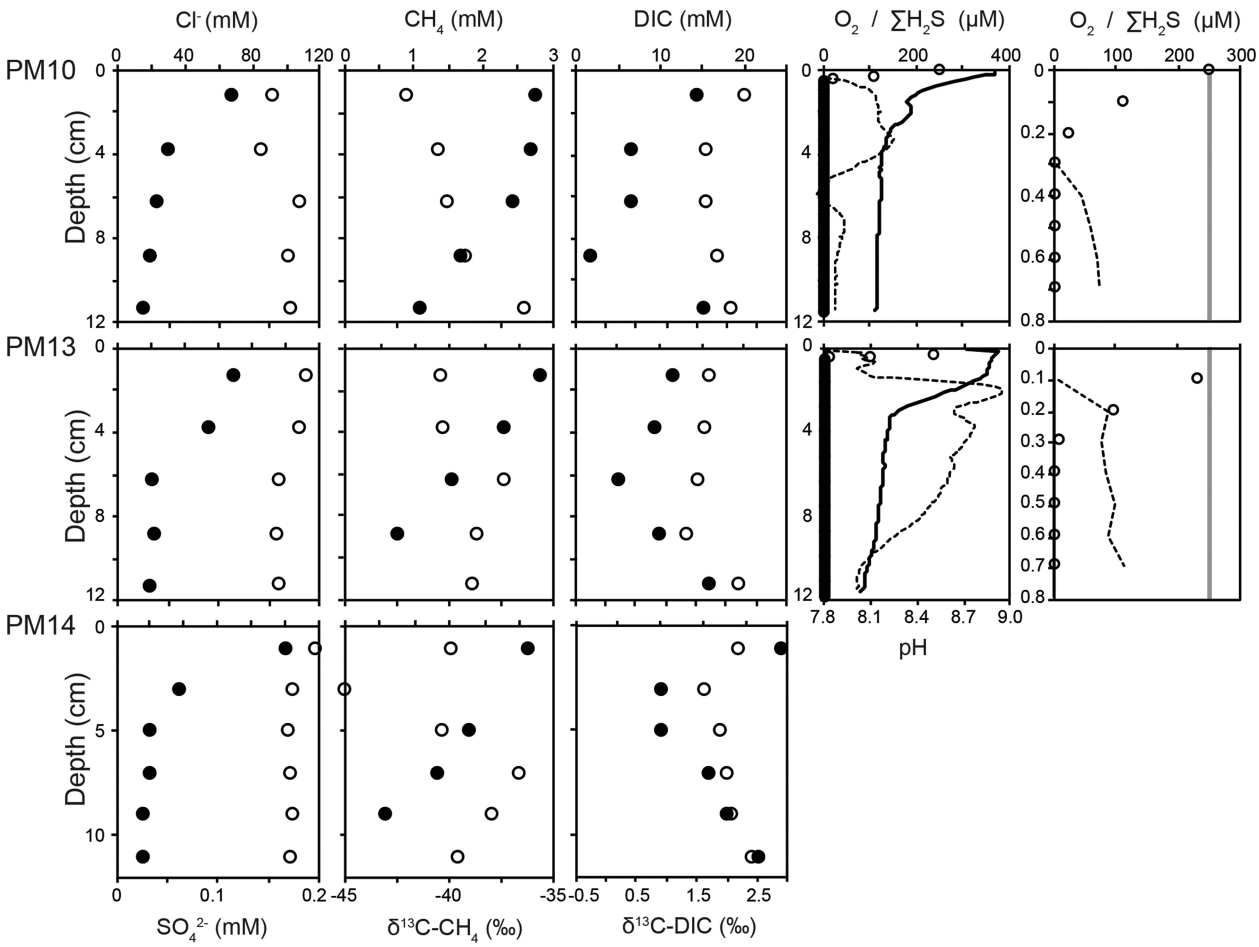

Figure 2. Geochemical profiles for the samples collected near the pool margin (stations PM10, PM13 and PM14). Open symbols and dashed line represent the concentrations referred to the top axis (chloride, methane, DIC, dissolved oxygen and sulfide), whereas solid symbols represent the concentrations and isotopic compositions referred to the bottom axis (sulfate, $\delta^{13}C$ values of methane and DIC, and pH). The profiles of dissolved sulfide and pH in the upper 0.8 cm were further magnified in the panels to the right for better visualization of the concentration variation near the air-fluid interface. The concentration of dissolved oxygen in equilibrium with the atmospheric oxygen under the *in situ* condition is marked with a gray line at 249.3 μM.

3.8×10^4 copies g^{-1} at station PP4 and 5.1×10^5 copies g^{-1} at station PP11. The high values of both genes occurred in the SMTZ and high methane zones.

DISCUSSION

Sources of fluids and microbial communities

Fluids and gases emanating from the bubbling features of MVs are generally considered to represent materials resembling characteristics of a deep source. A recent study based on the abundance of doubly substituted isotopologues ($^{13}CDH_3$ and $^{12}CD_2H_2$) indicated that methane discharged from this MV was generated by thermal maturation of organic matter at ~150°C (Rumble *et al.* 2018). Such a temperature estimate could be translated into a depth of ~6.3 km, assuming an average surface temperature of 24°C and a geothermal gradient of 20°C km^{-1} (Wu *et al.* 2013). This temperature or depth range for methane formation, however, exceeds the highest temperature (122°C) ever reported for microbial growth under laboratory conditions (Takai *et al.* 2008). This finding suggests that the gas/fluid source is sterilized by a local geothermal gradient and decoupled from the microbial source.

Mixing of deeply sourced, sterilized fluids with shallow, cell-containing groundwater appears to be the most plausible mechanism to explain the origin of the observed microbial communities. In this study, a total of 5.4–11.4% of the community members in two individual bubbling fluids were closely related to *Thermodesulfovibrio yellowstonii*, *Methanosaeta thermophila* and *Thermococcus mexicalis* (Fig. S5; Table S3, Supporting Information). Sequence analyzes further revealed that these sequences were nearly identical (≤2 bp difference) to the near full-length sequences affiliated (≥96% identity) with thermophiles and hyperthermophiles within these lineages obtained in a previous study (Cheng *et al.*, 2012). If these community members are truly thermophilic or hyperthermophilic, as inferred from sequence identity, they represent the deeply sourced components that contribute to the overall community assemblages. In addition, culture experiments have shown that these strains can grow at temperatures ranging between 30 and 105°C, with optimum growth temperatures between 55 and 100°C (Kamagata *et al.* 1992; Henry *et al.* 1994; Imachi *et al.* 2002; Lepage *et al.* 2004). If these potential thermophiles or hyperthermophiles proliferate at the corresponding optimum temperatures, they could have been introduced into the fracture network that is open to the input of groundwater from multiple depths between 1.5 and 3.8 km. Alternatively, temperatures ranging between 60

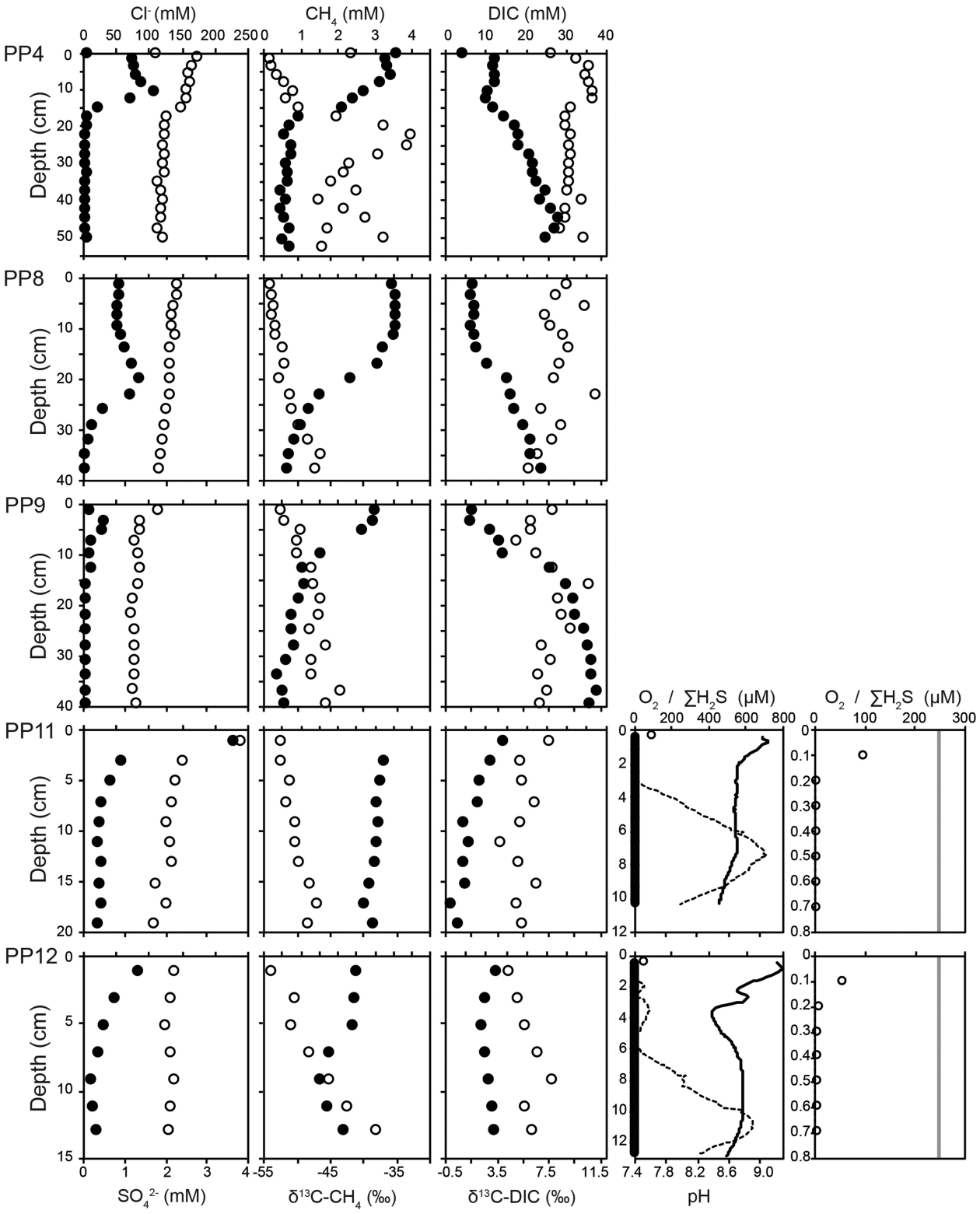

Figure 3. Geochemical profiles for the samples collected from the pool periphery (stations PP4, PP8, PP9, PP11 and PP12). Open symbols and dashed line represent the concentrations referred to the top axis (chloride, methane, DIC, dissolved oxygen and sulfide), whereas solid symbols represent the concentrations and isotopic compositions referred to the bottom axis (sulfate, $\delta^{13}C$ values of methane and DIC, and pH). The data points at zero depth of station PP4 represent BF2016. The profiles of dissolved sulfide and pH in the upper 0.8 cm were further magnified in the panels to the right for better visualization of the concentration variation near the air-mud interface. The concentration of dissolved oxygen in equilibrium with the atmospheric oxygen under the *in situ* condition is marked with a gray line at 249.3 μM.

Table 1. Fluxes[1,5] of dissolved oxygen, sulfide, sulfate and methane near the air-fluid/mud interface and across the concentration transition.

	Dissolved oxygen[2]		Sulfide[2]		Sulfate[3]		Methane[4]	
Station No.	Depth (cm)	Flux (mole m^{-2} d^{-1})	Depth (cm)	Flux (mole m^{-2} d^{-1})	Depth (cm)	Flux (mole m^{-2} d^{-1})	Depth (cm)	Flux (mole m^{-2} d^{-1})
Stations near the bubbling feature								
BF15	0.2–0.3	-2.06×10^{-2}	3.3–4.6	3.23×10^{-4}				
BF16	0.2–0.3	-2.05×10^{-2}	0.1–0.6	6.50×10^{-4}				
			5.4–7.6	6.79×10^{-4}				
BF17	0.1–0.2	-2.91×10^{-2}	0–1.4	1.07×10^{-3}				
			3.0–8.5	1.72×10^{-4}				
BF18	0–0.1	-2.38×10^{-2}	2.3–3.4	1.04×10^{-3}				
BF19	0–0.1	-2.81×10^{-2}	0.4–1.6	1.00×10^{-3}				
Stations near the pool margin								
PM10	0–0.1	-2.30×10^{-2}	0.3–0.4	4.60×10^{-3}	0–1.3	3.83×10^{-4}		
					1.3–3.8	-1.60×10^{-4}		
PM13	0.1–0.2	-2.08×10^{-2}	0.1–0.2	9.37×10^{-3}	0–1.3	3.68×10^{-4}		
					1.3–6.3	-1.02×10^{-4}		
PM14					0–1.0	8.71×10^{-4}		
					1.0–3.0	-3.42×10^{-4}		
Stations in the pool peripheral								
PP4					0–1.2	5.51×10^{-3}	1.2–10.1	7.09×10^{-4}
					5.7–10.1	5.51×10^{-4}	12.4–22.3	3.40×10^{-3}
					10.1–17.3	-1.18×10^{-3}		
PP8					0–1.0	4.97×10^{-3}	1.0–16.5	2.73×10^{-4}
					9.0–19.5	2.90×10^{-4}	19.5–37.3	5.64×10^{-4}
					19.5–31.5	-4.91×10^{-4}		
PP9					0–1.0	0	1.0–18.5	1.43×10^{-3}
					1.0–3.0	1.21×10^{-3}		
					3.0–7.0	-4.34×10^{-4}		
PP11	0–0.1	-1.82×10^{-2}	2.4–7.2	1.41×10^{-3}	0–1.0	1.74×10^{-2}	3.0–17.0	7.12×10^{-4}
			7.2–10.7	-1.39×10^{-3}	1.0–3.0	-6.94×10^{-3}		
PP12	0–0.1	-3.06×10^{-2}	5.3–10.3	1.34×10^{-3}	0–1.0	7.97×10^{-3}	1.0–12.7	2.53×10^{-3}
			10.3–12.4	-1.39×10^{-3}	1.0–3.0	-1.83×10^{-3}		

[1]Negative and positive fluxes indicate downward and upward transport, respectively.
[2]Fluxes of dissolved oxygen and sulfide were calculated for near the air–fluid/mud interfaces at all stations with available data. Fluxes of sulfide were additionally calculated for the deeper intervals below the sulfate-depletion zone in the pool peripheral.
[3]Fluxes of sulfate were calculated for stations near the pool margin and in the pool peripheral where downward decreasing sulfate gradients in the upper portion of cored mud were clear and mud content was greater. Additional calculations were performed for the top few centimeters at stations PP4, PP8 and PP9 where downward increasing sulfate gradients were observed.
[4]Fluxes of methane were calculated only for stations in the pool peripheral because methane is highly mobile and the gradient could be easily disturbed by the bubbling agitation.
[5]Diffisivities for different ions or molecules are adapted from Tse and Sandall (1979), Krom and Berner (1980), Iversen and Jørgensen (1993) and Tamimi *et al.* (1994).

and 70°C could enable the proliferation of the potential thermophiles. The microbial communities could have originated from a source at depths equivalent to this temperature range (1.8–2.3 km deep). Overall, these deeply sourced, cell-free fluids mixed with groundwater inherited with thermophilic and mesophilic communities ascend to land surface, thereby providing an abundant supply of electron donors, reducing power and microbial seeds to shape redox transitions and biogeochemical processes near the surface of the MV ecosystem.

Surface abiotic processes and redox transition

Our results indicated that chloride concentrations of the top fluids increased from 93–102 mM near the bubbling features to 92–118 mM near the pool margin and 116–239 mM in the pool periphery. Such a progressive increase of chloride concentration suggests a decreasing frequency of the submergence of mud beneath fluids and an increasing frequency of exposure to the atmosphere as the distance from the bubbling feature increases. Since chloride is inert to biological and most abiotic reactions, the variation pattern combined with the negative correlation between chloride and water content (Fig. S6, Supporting Information) further suggests that evaporation plays a role in increasing solute concentration.

Similar variations were observed for sulfate, with low concentrations (≤110 μM) occurring near the bubbling feature and high concentrations (up to 3.59 mM) in the pool periphery. Like chloride, sulfate concentrations were also negatively correlated with water content (Fig. S6, Supporting Information). The pattern of solute enhancement is, however, not exactly the same between chloride and sulfate. If the chloride concentration of the bubbling fluids is considered the source characteristic, evaporation could lead to chloride enrichment in the pool periphery by a factor of 1.3–2.6 (with the exception of station PP9). For comparison, the enrichment factor of sulfate ranged from 7.7 to 89.8 (with the exception of station PP9). The differential enrichment of solutes suggests that an additional source of sulfate is required. The concentrations of top dissolved sulfide in the pool

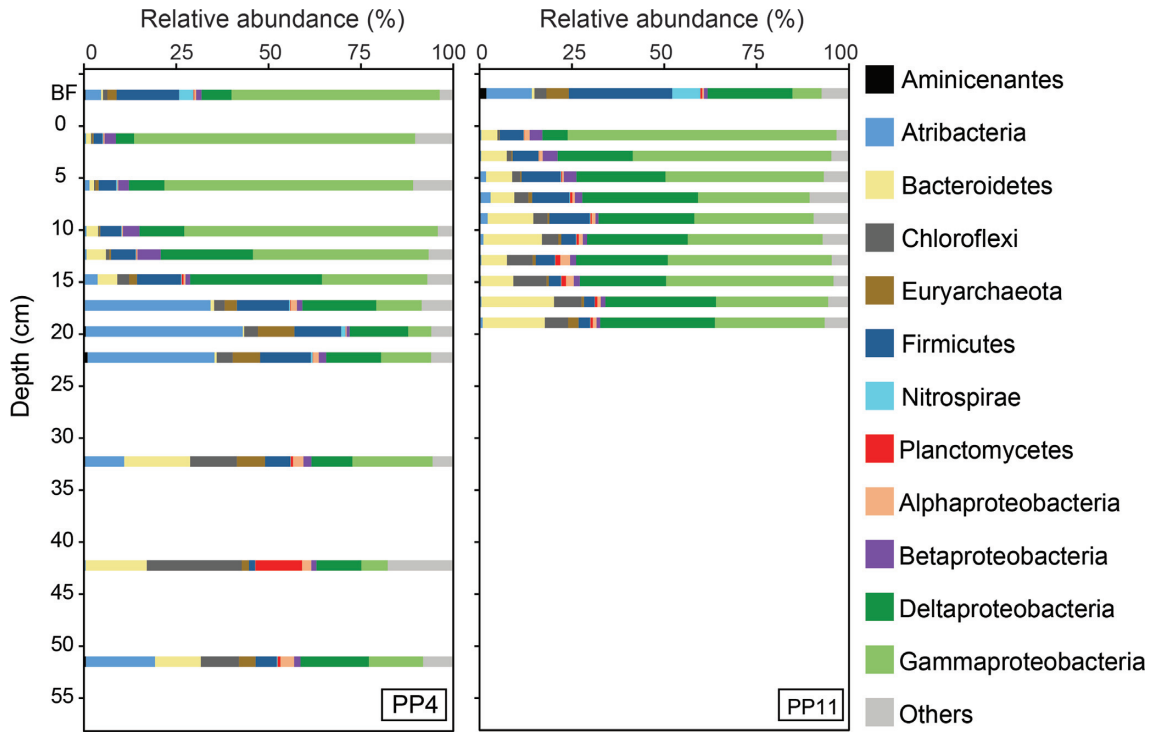

Figure 4. Phylum/class-based community compositions for stations PP4 and PP11.

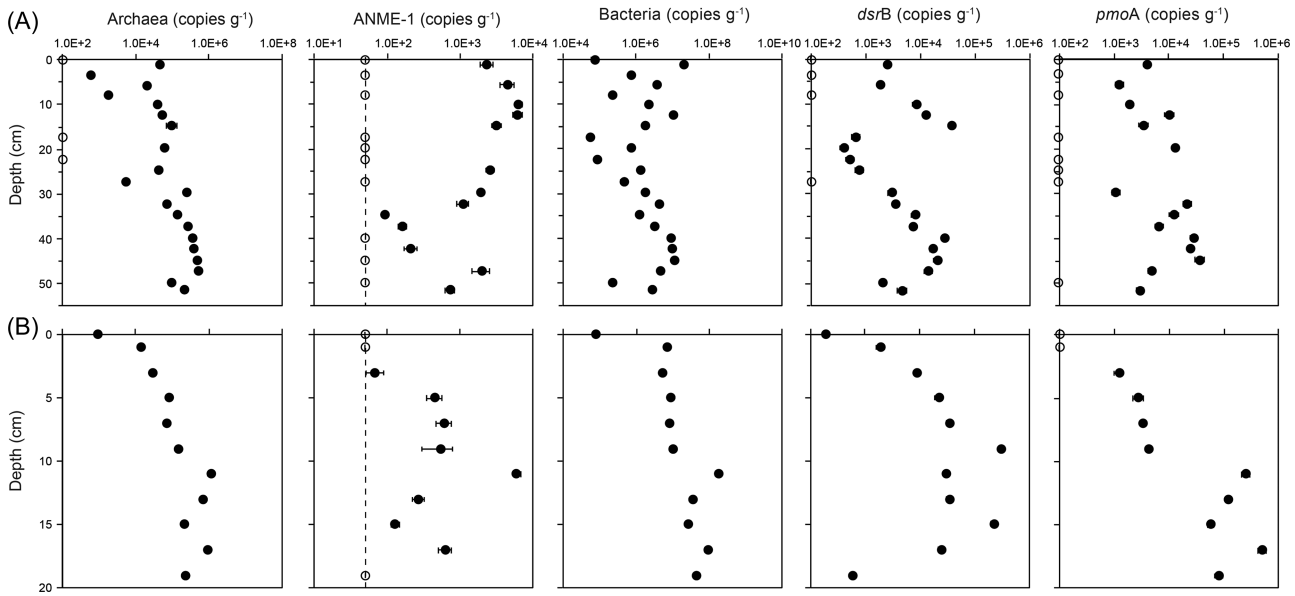

Figure 5. Profiles of gene copy numbers for stations PP4 (A) and PP11 (B). Data points at zero depth represent gene copy numbers for samples collected from the bubbling features. Analyzed genes and taxonomic groups include 16S rRNA genes for bacterial, archaeal and ANME-1 members, *dsrB* genes and *pmo*A genes. Open circles and dashed line represent the copy number below the limit of detection (either 50 or 100 copies g^{-1}). The uncertainty of analysis represents one standard deviation of quadruple replicates.

periphery were comparable to those in the pool or near the pool margin and far less than those of top sulfate (Figs 1–3). Pyrite was detected throughout the cored muds. In this regard, instead of dissolved sulfide, the oxidation of pyrite with the production of sulfuric acid is perhaps the best explanation for such large increases in sulfate levels at the air-mud interface. Although abiotic oxidation of pyrite under atmospheric conditions is generally considered to be slow (Balci *et al.* 2007), whether abiotic or microbial oxidation accounts for the observed accumulation of sulfate remains uncertain. Furthermore, the oxidation of pyrite could have proceeded with the consumption of oxygen, thereby contributing to oxygen depletion, as was observed in the present study (Figs 1–3 and Discussion section). Overall, pyrite oxidation is needed to charge the surface sediments with millimolar sulfate and convert sediments to anoxic conditions, both of which provide environmental contexts that are favorable for the development of anaerobic metabolism.

The profiles of dissolved oxygen were all similar regardless of the site category or geochemical characteristics. In addition, oxygen supersaturation was not observed near the air-fluid/mud interface, suggesting that photosynthetic production of oxygen was limited, probably because of substantial light attenuation caused by suspended muds and oily patches. The diffusive fluxes of dissolved oxygen were calculated to span from 18.2 to 30.6 mmol m^{-2} d^{-1} (Table 1). Since gas bubbling agitated pool fluids vigorously and the measurements were carried out in the static mode off site, the derived flux represents the minimum value for the bubbling feature, but would more closely mimic the true value for the station near the pool margin or in the pool periphery. This range was comparable with most values (10–200 mmol m^{-2} d^{-1}) reported for deep marine cold seeps and MVs (Boetius and Wenzhöfer 2013), and suggests that the reducing power was strong enough to confine the oxygen penetration within the upper few millimeters. Dissolved sulfide might serve as a reductant for oxygen depletion. Among all stations, upward sulfide fluxes near the air-fluid/mud interface at five stations (BF16, BF17, BF19, PM10 and PM13) ranged between 0.65 and 9.37 mmol m^{-2} d^{-1} (Table 1). Given that the stoichiometric ratio of sulfide to oxygen is 0.5 for sulfide oxidation:

$$HS^- + 2O_2 \rightarrow SO_4^{2-} + H^+ \quad (2)$$

The upward reducing power of sulfide within the upper 1 cm of fluids/muds constitutes 6.3–90.1% of the downward oxygen fluxes. Since the upward sulfide gradient occurred at depths where dissolved oxygen was still present, microbial and abiotic oxidation of dissolved sulfide contributed both to the consumption of dissolved oxygen and production of sulfate. Certainly, other reductants, such as methane expelled into the pool or produced *in situ*, and pyrite and organic matters associated with emanated muds also play a role in the consumption of oxygen. For example, upward fluxes of methane in the upper sediments at the pool periphery stations ranged between 0.27 and 2.53 mmol m^{-2} d^{-1}. If the downward fluxes of dissolved oxygen at these stations were similar to those at other stations in the pool periphery, the upward methane fluxes contributed 2.2–16.6% of equivalent reducing power. Similarly, upward sulfate fluxes near the air-mud interface of stations PP4, PP8, PP11 and PP12 ranged between 4.97 and 17.4 mmol m^{-2} d^{-1}. As discussed earlier, these fluxes or concentration gradients were generated by pyrite oxidation. Using the stoichiometric ratio of O_2 to sulfate (15/8), pyrite oxidation contributed 38.2−179.2% of equivalent reducing power.

Biogeochemical processes and community compositions

To further address potential metabolic reactions across redox gradients, the geochemical characteristics susceptible to microbial processes and 16S rRNA gene sequences affiliated with specific lineages (orders/families/genera) were integrated. In addition to using geochemical characteristics, potential metabolic reactions of specific community members were also inferred on the basis of high sequence identity to known strains and common metabolisms shared among most or all members within specific lineages. We note that sequence analyzes do not necessarily recover the thorough diversity and predict functional capacity and activity of the microbial community.

Our combined data indicated that some aerobic metabolisms were active in the pool and contributed to the production of CO_2. For example, $\delta^{13}C$ values of methane and DIC from a depth of 7.5 cm at station BF19 were −30‰ and −1.2‰, respectively. These values were distinct from those of methane (greater) and DIC (less) from the bubbling fluid, suggesting the presence of active methanotrophy. Whether such spotty methanotrophic activities were aerobic or anaerobic remains uncertain, as the relative abundance of methanotrophs affiliated with *Methylomicrobium* and the ANME-1 lineage were only around 0.1 and 0.5%, respectively (Fig. 4; Table S2, Supporting Information). Furthermore, a high proportion of community members (21–57%) were affiliated with heterotrophs that were taxonomically assigned to the Gamma- and Delta- subdivisions of Proteobacteria (including Alcanivoracaceae, Alteromonadaceae, Pseudomonadaceae, *Smithella* spp. and Syntrophorhabdaceae) (Yakimov *et al.* 1998; López-Pérez and Rodriguez-Valera 2014; Tan, Nesbø and Foght 2014; Jayamani and Cupples 2015). Although the exact organic entities degraded by these microorganisms were not clear, the abundance of these heterotrophs was high in the bubbling fluid (57% for BF2016 and 20% for BF16–2.5 cm) and the top mud (53% for station PP4 and 59% for station PP11), and decreased with increasing depth (Fig. 4). This distribution pattern suggests their physiological preference for habitats where oxygen is accessible.

Despite aerobic respiratory metabolism, anaerobic processes also play a role in community functions in the mud pool. In particular, the lowest $\delta^{13}C$ values of methane were around −42‰, a value that is 7‰ more negative than those of the bubbling fluid and suggests the role of *in situ* methanogenesis. For comparison, a total of 0.1–4.0% of sequences related to Methanosaetaceae, Methanobacteriaceae and Methanoregulaceae were detected. Previous incubation experiments also indicated that methanogens exploiting acetate, methyl compounds and CO_2 were all viable in this MV (Cheng *et al.* 2012). These results suggest that transient *in situ* methanogenesis could have generated methane at quantities that were sufficient to create a patchy distribution of distinct isotopic compositions of methane.

The geochemical results suggest a transitional pattern from one end component (the pool) that was highly impacted by the advection supply of deeply sourced fluids and gases, to the other end component (the pool periphery) modulated by surface evaporation and oxidation processes and subsurface microbial processes. Therefore, only the biogeochemical processes in the pool periphery comprise the focus of further discussion.

The geochemical pattern of mud columns in the pool periphery marked a SMTZ, indicating stratified distribution of sulfate reduction, anaerobic oxidation of methane and methanogenesis (Iversen and Jørgensen 1985; Parkes *et al.* 2007; Leloup *et al.* 2009). Whereas such a geochemical pattern is analogous to marine counterparts, there is one major difference such that the maximum sulfate concentrations were not always observed at the top in the terrestrial MV. In marine seeps or MVs, seawater sulfate acts as an infinitely large reservoir to fuel subsurface sulfate reducers through downward diffusion. In this study, sulfate concentrations increased from ~0.9 mM at the top, to above 1.4 mM at 10 cm of station PP4, and 20 cm of station PP8, a depth range where oxygen was scarce. As barite and gypsum were absent and dissolved sulfide was not high, the increase of sulfate in the anoxic zone is best explained by the microbial oxidation of sulfur-bearing minerals (Lovley and Phillips 1994; Weber, Thamdrup and Habicht 2016; Wasmund, Mußmann and Loy 2017). In addition to the anoxic production of sulfate, the sulfate-depletion zone was underlain by a zone of increased sulfide levels at stations PP9, PP11 and PP12. The segregation of the

sulfide maximum from the largest downward sulfate gradient suggests sequestration of dissolved sulfide by iron oxyhydroxide, and cryptic sulfur cycling at the base of the sulfate reduction zone.

The geochemical interpretation regarding sulfur metabolism (sulfate reduction and sulfur oxidation) is supported by 16S rRNA gene screening and qPCR results. Our analyzes indicated that sequences related to a number of sulfur-oxidizing bacteria mainly affiliated with Ectothiorhodospiraceae and *Thioalkalispira* spp. within Gammaproteobacteria and *Desulfurivibrio alkaliphilus* within Deltaproteobacteria, and sulfate-reducing bacteria mainly affiliated with *Desulfatitalea* spp. within Deltaproteobacteria were detected throughout the cored muds (Fig. 4; Table S2, Supporting Information). The abundance of *dsrB* genes either peaked or increased to a high level in the sulfate-depletion zone (Fig. 5). The sulfur-oxidizing bacteria described above have been reported to oxidize various forms of reduced sulfur (e.g. sulfide, thiosulfate and elemental sulfur) under oxic conditions, or with nitrate under anoxic conditions (Sorokin et al., 2001, 2002; Melton *et al.* 2016; Thorup *et al.* 2017). The likelihood of cable bacteria in long-ranging electron transport is rejected, as (1) the proton gradient measured in this study was only ~1.2 units; (2) sequences related to known cable bacteria were absent and (3) the distance from the sulfide maximum to the pH maximum was far greater than that ever reported for the development of cell chains (Pfeffer *et al.* 2012). Furthermore, the coexistence of abundant microorganisms that are capable of catalyzing oxidative and reductive pathways at low-sulfate depths suggests that sulfur has to be rapidly cycled between the oxidized and reduced forms.

The complementary variation between the concentration and isotopic composition of methane suggests the presence of anaerobic oxidation of methane underlain by methanogenesis. This interpretation is corroborated by the ^{13}C-depleted DIC in the low-methane zone and the ^{13}C-enriched DIC in the high methane zone. Geochemical inferences were also supported by gene screening, through which sequences related to ANME-1 members and methanogens using CO_2 and acetate (Methanobacteriaceae and Methanosaetaceae) were detected. In addition, the copy numbers of ANME-1 members increased by a factor of 10 between the SMTZ and adjacent methanogenic or sulfate reduction zones. Assuming that archaeal communities were only composed of methanogens and anaerobic methanotrophs (based on sequence data), gene copy numbers of methanogens would peak in or near the methanogenic zone. The efficiency of these methanotrophs in consuming methane (76% of methane removal based on flux comparison) is high and similar to those of marine counterparts (Boetius and Wenzhöfer 2013). The flux calculation also indicated various ratios of upward methane fluxes to downward sulfate fluxes across the SMTZ at different stations, suggesting various degrees of the dependence of anaerobic oxidation of methane on sulfate reduction.

In addition to metabolisms discussed above, the abundance of sequences related to type I aerobic methanotrophs (mainly affiliated with *Methylomicrobium* spp.) and methylotrophs increased at depths greater than 10 cm, where oxygen was scarce. Such a distribution pattern is comparable with the qPCR results, in which *pmoA* gene copy numbers peaked at 40 cm at station PP4, and at 17.5 cm at station PP11, and showed a substantial decline above the SMTZ (Fig. 5). The increased abundance of these community members known to oxidize either methane or methyl compounds with the consumption of oxygen in the anoxic zone is unexpected. One possibility is that the increased abundance of methanotrophs and methylotrophs represent the residue community members that once flourished on/near the surface where oxygen was available, but were later buried by sediment deposition. Alternatively, these methanotrophs possess metabolic flexibility, as they can exploit electron acceptors other than oxygen (e.g. nitrate) (Kits, Klotz and Stein 2015). Current data are not conclusive to assert any possibility.

Long-term geological control on microbial community and dispersal

Despite community changes associated with transient and dynamic perturbations near the surface on a contemporary time scale, the effects of long-term (million-year scaled) geological processes were also investigated. The principle stems from the fact that the formation (Kutingkeng) hosting the investigated MV was formed in the outer continental shelf during the Pliocene-Pleistocene and was progressively accreted and exhumed above sea level by the late fault activity driven by subduction of the Eurasian plate (Teng and Lin, 2004; Chen *et al.* 2017). Under this tectonic framework, current sediments in the South China Sea and offshore southwestern Taiwan represent the modern analog of Pliocene-Pleistocene sediments hosting the SYNHMV. To address this scenario, published community compositions recovered from cores distributed in the South China Sea (Lin *et al.* 2014; Graw *et al.* 2018) were merged with the data reported in the present study. Community dissimilarity (Bray-Curtis) was computed and visualized using principle coordinate analysis (PCoA). The assessment was based on the assumption that microbial communities in current South China Sea sediments are the same as those in the geological past. The analysis only incorporated studies with sequences that overlapped the same hypervariable regions. Therefore, limited spatial resolution (three sites from the abyssal plain and one site from the continental slope) was noted.

Our analyzes showed that community compositions were distinct between individual site categories (abyssal plain, continental slope and terrestrial MV; Fig. 6). In addition to site variance, communities also varied by metabolic categorization (sulfate reduction versus methanogenesis) to a lesser degree, suggesting that different combinations of community members could lead to similar community functions. Detailed sequence analyzes for individual OTUs indicated that greater fractions of sequences or OTUs were shared between communities in individual site categories or in marine versus terrestrial environments (Fig. 6). A total of 1535 out of 41 953 and 3561 out of 42 395 OTUs were shared between communities in the abyssal plain and terrestrial MV, respectively. The numbers of shared OTUs were reduced to 299 (out of 56 001) for all marine sediments and nine (out of 97 935) when all marine and terrestrial samples were considered. These nine persistent OTUs were more abundant in the continental slope (site MD3280) and at sites U1432 and U1433 (2–7% of sequences), less abundant at site U1431 (0.6%) and least abundant in the terrestrial MV (0.01–0.04%). Sequences of these persistent OTUs were classified in Elusimicrobia, Lokiarchaeota, Hadesarchaea, Chloroflexi, Bacteroidetes, Actinobacteria and Deltaproteobacteria (Table S4, Supporting Information). These results are partly comparable with the community pattern commonly recovered from marine sediments at depths of up to 100 m around the globe (Petro *et al.* 2017). One notable discrepancy was observed among Atribacteria-related members. Although diverse and abundant Atribacteria-related OTUs were

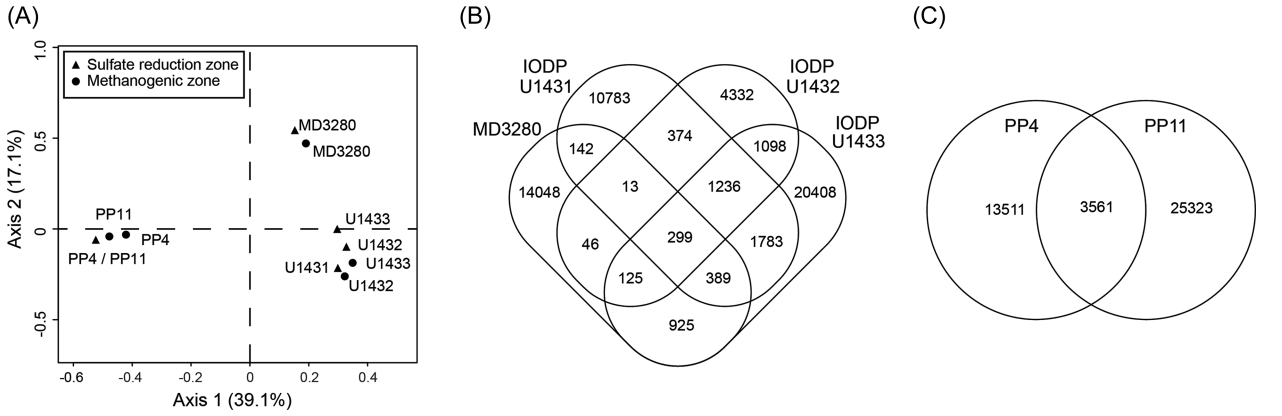

Figure 6. (A) Variance of community compositions for marine sediments from the South China Sea (MD3280 from Lin *et al.* (2014) and IODP U1431–U1433 from Graw *et al.* (2018)) and SYNHMV (this study). Venn diagrams comparing the numbers of OTUs shared between sites in (B) the South China Sea and (C) SYNHMV. The community variance was deduced by principal coordinate analysis (PCoA) based on the Bray-Curtis dissimilarity for obtained 16S rRNA gene sequences. To maximize the numbers of persistent OTUs shared between sites, no sequence resampling was applied.

detected, all were confined to either marine or terrestrial environments. For example, OTU00002 in Table S2 (Supporting Information) was present in all terrestrial samples and constituted 2.4% of total sequences, but was absent in marine sediments. Overall, the present results suggest that these persistent members likely survive the stress imposed by diagenetic processes (e.g. burial, compaction and cementation), tectonic accretion and fault displacement, all of which account for the emplacement of sediments from marine into terrestrial environments over a time scale of millions of years. Analyzes of more samples at a higher spatial resolution and single-cell genomes are warranted to address the dispersal and selection mechanisms of microbial seedbanks across marine and terrestrial realms.

CONCLUSIONS

Geochemical and molecular characterization of samples retrieved from different compartments of the SYNHMV indicated a steep redox transition, with oxygen penetration being confined to the upper 4 mm of pool fluids or muds in the pool periphery. Flux calculations indicate that the oxidation of dissolved sulfide and pyrite is an important driver for oxygen consumption at the air-fluid/mud interface. The steep oxygen gradient was underlain by the compartmentalization of anaerobic metabolic reactions, including sulfur oxidation, sulfate reduction, anaerobic oxidation of methane and methanogenesis along the depth of the pool periphery. Such metabolic zonation and organization facilitates the efficient consumption of upward-migrating methane produced *in situ*. Furthermore, potential aerobic methylotrophs and methanotrophs were more abundant at depths devoid of oxygen, revealing a distribution pattern that contradicts their most common physiological preference for oxygen, and suggesting either alternative electron acceptors or a persistent population that was once proliferating in the oxic zone. Our results demonstrate that the reducing, sterilized fluids originating from great depths were seeded with microbial populations during upward transport along the fracture network. These microorganisms formed a metabolic architecture that drove the intensive cycling of sulfur, methane and organic carbon along redox transitions, thereby altering the physical and chemical contexts of the mud pool and pool periphery.

SUPPLEMENTARY DATA

Supplementary data are available at FEMSEC online.

ACKNOWLEDGMENTS

We are grateful to Dr. Shih-Hsiung Liang of National Kaohsiung Normal University for providing the lab space and facilities for microelectrode measurement and sample processing, Lu-Yu Wang for assistance in qPCR and sequence analyzes and Technology Commons, and Computer and Information Networking Center of National Taiwan University for technical support. We acknowledge the constructive and thorough comments provided by the reviewers and editor.

FUNDING

This work was supported by Taiwanese Ministry of Science and Technology (grant number 106–2116-M-002–025, 106–2116-M-002–002 and 107–2116-M-002–024) and Ministry of Education (Higher Education Sprout Project for NTU Research Center for Future Earth 107L901002).

Conflicts of interest. None declared.

REFERENCES

Balci N, Shanks WC,, III, Mayer B *et al.* Oxygen and sulfur isotope systematics of sulfate produced by bacterial and abiotic oxidation of pyrite. *Geochim Cosmochim Ac* 2007;**71**:3796–811.

Boetius A, Wenzhöfer F. Seafloor oxygen consumption fuelled by methane from cold seeps. *Nat Geosci* 2013;**6**:725–34.

Bray JR, Curtis JT. An ordination of the upland forest communities of southern Wisconsin. *Ecol Monogr* 1957;**27**:325–49.

Canfield DE, Raiswell R, Westrich JT *et al.* The use of chromium reduction in the analysis of reduced inorganic sulfur in sediments and shales. *Chem Geol* 1986;**54**:149–55.

Chang Y-H, Cheng T-W, Lai W-J *et al.* Microbial methane cycling in a terrestrial mud volcanoin eastern Taiwan. *Environ Microbiol* 2012;**14**:895–908.

Chao S, Sederoff R, Levings CS. Nucleotide sequence and evolution of the 18S ribosomal RNA gene in maize mitochondria. *Nucleic Acids Res* 1984;**12**:6629–44.

Chen N-C, Yang TF, Hong W-L *et al.* Production, consumption, and migration of methane inaccretionary prism of southwestern Taiwan. *AGU Publ* 2017;**18**:2970–89.

Cheng T-W, Chang Y-H, Tang S-L *et al.* Metabolic stratification driven by surface and subsurface interactions in a terrestrial mud volcano. *ISME J* 2012;**6**:2280–90.

Costello AM, Lidstrom ME. Molecular characterization of functional and phylogenetic genes from natural populations of methanotrophs in lake sediments. *Appl Environ Microb* 1999;**65**:5066–74.

Dimitrov LI. Mud volcanoes—the most important pathway for degassing deeply buried sediments. *Earth-Sci Rev* 2002;**59**:49–76.

Edgar RC, Haas BJ, Clemente JC *et al.* UCHIME improves sensitivity and speed of chimera detection. *Bioinformatics* 2011;**27**:2194–200.

Faith DP. Conservation evaluation and phylogenetic diversity. *Biol Conserv* 1992;**61**:1–10.

Geets J, Borremans B, Diels L *et al. DsrB* gene-based DGGE for community and diversity surveys of sulfate-reducing bacteria. *J Microbial Meth* 2006;**66**:194–205.

Graw M, D'Angelo G, Borchers M *et al.* Energy gradients structure microbial communities across sediment horizons in deep marine sediments of the South China Sea. *Front Microbiol* 2018;**9**:729.

Henry EA, Devereux R, Maki JS *et al. Thermodesulfovibrio yellowstonii*, gen. nov. and sp. nov.: its phylogenetic relationship to *Thermodesulfobacterium commune* and their origins deep within the bacterial domain. *Arch Microbiol* 1994;**161**:62–9.

Hill MO. Diversity and evenness: a unifying notation and its consequences. *Ecology* 1973;**54**:427–32.

Imachi H, Sekiguchi Y, Kamagata Y *et al. Pelotomaculum thermopropionicum* gen. nov., sp. nov., an anaerobic, thermophilic, syntrophic propionate-oxidizing bacterium. *Int J Syst Evol Micr* 2002;**52**:1729–35.

Iversen N, Jørgensen BB. Anaerobic methane oxidation rates at the sulfate-methane transition in marine sediments from Kattegat and Skagerrak (Denmark). *Limnol Oceanogr* 1985;**30**:944–55.

Iversen N, Jørgensen BB. Diffusion coefficients of sulfate and methane in marine sediments: influence of porosity. *Geochim Cosmochim Ac* 1993;**57**:571–8.

Jayamani I, Cupples AM. Stable isotope probing reveals the importance of *Comamonas* and *Pseudomonadaceae* in RDX degradation in samples from a navy detonation site. *Environ Sci Pollut R* 2015;**22**:10340–50.

Kallmeyer J, Pockalny R, Adhikari RR *et al.* Global distribution of microbial abundance and biomass in subseafloor sediment. *P Natl Acad Sci USA* 2012;**109**:16213–6.

Kamagata Y, Kawasaki H, Oyaizu H *et al.* Characterization of three thermophilic strains of *Methanothrix* ("*Methanosaeta*") *thermophila* sp. nov. and Rejection of *Methanothrix* ("*Methanosaeta*") *thermoacetophila*. *Int J Syst Evol Micr* 1992;**42**:463–8.

Khripounoff A, Caprais JC, Decker C *et al.* Variability in gas and solute fluxes through deep-sea chemosynthetic ecosystems inhabited by vesicomyid bivalves in the Gulf of Guinea. *Deep-Sea Res Pt I* 2015;**95**:122–30.

Kits KD, Klotz MG, Stein LY. Methane oxidation coupled to nitrate reduction under hypoxia by the Gammaproteobacterium *Methylomonas denitrificans*, sp. nov. type strain FJG1. *Environ Microbiol* 2015;**17**:3219–32.

Krom MD, Berner RA. The diffusion coefficients of sulfate, ammonium, and phosphate ions in anoxic marine sediments. *Limnol Oceanogr* 1980;**25**:327–37.

Leloup J, Fossing H, Kohls K *et al.* Sulfate-reducing bacteria in marine sediment (Aarhus Bay, Denmark): abundance and diversity related to geochemical zonation. *Environ Microbiol* 2009;**11**:1278–91.

Lepage E, Marguet E, Geslin C *et al.* Molecular diversity of new Thermococcales isolates from a single area of hydrothermal deep-sea vents as revealed by randomly amplified polymorphic DNA fingerprinting and 16S rRNA gene sequence analysis. *Appl Environ Microb* 2004;**70**:1277–86.

Lin L-H, Wu L-W, Cheng T-W *et al.* Distributions and assemblages of microbial communities along a sediment core retrieved from a potential hydrate-bearing region offshore southwestern Taiwan. *J Asian Earth Sci* 2014;**92**:276–92.

Lipp JS, Morono Y, Inagaki F *et al.* Significant contribution of Archaea to extant biomass in marine subsurface sediments. *Nature* 2008;**454**:991–4.

Lovley DR, Phillips EJ. Novel processes for anaerobic sulfate production from elemental sulfur by sulfate-reducing bacteria. *Appl Environ Microb* 1994;**60**:2394–9.

López-Pérez M, Rodriguez-Valera F. The family *Alteromonadaceae*. In: DeLong EF , Lory S , Stackebrandt E *et al.* (eds). *The Prokaryotes*. Berlin, Heidelberg: Springer, 2014, 69–92.

Mazzini A, Etiope G. Mud volcanism: an updated review. *Earth-Sci Rev* 2017;**168**:81–112.

McMahon S, Parnell J. Weighing the deep continental biosphere. *FEMS Microbiol Ecol* 2014;**87**:113–20.

Melton ED, Sorokin DY, Overmars L *et al.* Complete genome sequence of *Desulfurivibrio alkaliphilus* strain AHT2T, a haloalkaliphilic sulfidogen from Egyptian hypersaline alkaline lakes. *Stand Genomic Sci* 2016;**11**:67.

Nisbet EG, Sleep NH. The habitat and nature of early life. *Nature* 2001;**409**:1083–91.

Onstott TC, Phelps TJ, Kieft T *et al.* A global perspective on the microbial abundance and activity in the deep subsurface. In: Seckbach J (ed). *Enigmatic Microorganisms and Life in Extreme Environments*. Dordrecht: Springer, 1998, 489–99.

Parada AE, Needham DM, Fuhrman JA. Every base matters: assessing small subunit rRNA primers for marine microbiomes with mock communities, time series and global field samples. *Environ Microbiol* 2016:**18**:1403–14

Parkes RJ, Cragg BA, Banning N *et al.* Biogeochemistry and biodiversity of methane cycling in subsurface marine sediments (Skagerrak, Denmark). *Environ Microbiol* 2007;**9**:1146–61.

Petro C, Starnawski P, Schramm A *et al.* Microbial community assembly in marine sediments. *Aquat Microb Ecol* 2017;**79**:177–95.

Pfeffer C, Larsen S, Song J *et al.* Filamentous bacteria transport electrons over centimetre distances. *Nature* 2012;**491**:218–21.

Rumble D, Ash JL, Wang PL *et al.* Resolved measurement of $^{13}CDH_3$ and $^{12}CD_2H_2$ from a Taiwan mud volcano. *J Asian Earth Sci* 2018 (in press). https://doi.org/10.1016/j.jseaes.2018.03.007

Schloss PD, Westcott SL, Ryabin T *et al.* Introducing mothur: open-source, platform-independent, community-supported software for describing and comparing microbial communities. *Appl Environ Microb* 2009;**75**:7537–41.

Schloss PD, Westcott SL. Assessing and improving methods used in operational taxonomic unit-based approaches for 16S rRNA gene sequence analysis. *Appl Environ Microb* 2011;**77**:3219–26.

Sorokin DY, Lysenko AM, Mityushina LL *et al*. *Thioalkalimicrobium aerophilum* gen. nov., sp. nov. and *Thioalkalimicrobium sibericum* sp. nov., and *Thioalkalivibrio versutus* gen. nov., sp. nov., *Thioalkalivibrio nitratis* sp.nov., novel and *Thioalkalivibrio denitrificancs* sp. nov., novel obligately alkaliphilic and obligately chemolithoautotrophic sulfur-oxidizing bacteria from soda lakes. *Int J Syst Evol Microbiol* 2001;**51**:565–80.

Sorokin DY, Tourova TP, Lysenko AM *et al*. *Thioalkalivibrio thiocyanoxidans* sp. nov. and *Thioalkalivibrio paradoxus* sp. nov., novel alkaliphilic, obligately autotrophic, sulfur-oxidizing bacteria capable of growth on thiocyanate, from soda lakes. *Int J Syst Evol Microbiol* 2002;**52**:657–64.

Starnawski P, Bataillon T, Ettema TJG *et al*. Microbial community assembly and evolution in subseafloor sediment. *P Natl Acad Sci* 2017;**114**:2940–5.

Takai K, Nakamura K, Toki T *et al*. Cell proliferation at 122°C and isotopically heavy CH_4 production by a hyperthermophilic methanogen under high-pressure cultivation. *P Natl Acad Sci USA* 2008;**105**:10949–54.

Tamimi A, Rinker EB, Sandall OC. Diffusion coefficients for hydrogen sulfide, carbon dioxide, and nitrous oxide in water over the temperature range 293–368 K. *J Chem Eng Data* 1994;**39**:330–2.

Tan B, Nesbø C, Foght J. Re-analysis of omics data indicates *Smithella* may degrade alkanes by addition to fumarate under methanogenic conditions. *ISME J* 2014;**8**:2353–6.

Teng L-S, Lin A-T. Cenozoic tectonics of the China continental margin: insights from Taiwan. *Geo Soc Lond Spec Publ* 2004;**226**:313–32.

Thorup C, Schramm A, Findlay AJ *et al*. Disguised as a sulfate reducer: growth of the Deltaproteobacterium *Desulfurivibrio alkaliphilus* by sulfide oxidation with nitrate. *mBio* 2017;**8**:e00671–17.

Tse FC, Sandall OC. Diffusion coefficient for oxygen and carbon dioxide in water at 25°C by unsteady state desorption from a quiescent liquid. *Chem Eng Commun* 1979;**3**:147–53.

Tu T-H, Wu L-W, Lin Y-S *et al*. Microbial community composition and functional capacity in a terrestrial ferruginous, sulfate-depleted mud volcano. *Front Microbiol* 2017;**8**:2137.

Thomson J, Higgs NC, Croudace IW *et al*. Redox zonation of elements at an oxic/post-oxic boundary in deep-sea sediments. *Geochim Cosmochim Ac* 1993;**57**:579–95.

Wang P-L, Chiu Y-P, Cheng T-W *et al*. Spatial variations of community structures and methane cycling across a transect of Lei-Gong-Hou mud volcanoes in eastern Taiwan. *Front Microbiol* 2014;**5**:2946.

Wasmund K, Mußmann M, Loy A. The life sulfuric: microbial ecology of sulfur cycling in marine sediments. *Environ Microbiol Rep* 2017;**9**:323–44.

Weber HS, Thamdrup B, Habicht KS. High sulfur isotope fractionation associated with anaerobic oxidation of methane in a low-sulfate, iron-rich environment. *Front Earth Sci* 2016;**4**:243.

Whitman WB, Coleman DC, Wiebe WJ. Prokaryotes: the unseen majority. *P Natl Acad Sci USA* 1998;**95**:6578–83.

Wu S-K, Chi W-C, Hsu S-M *et al*. Shallow crustal thermal structures of central taiwan foothills region. *Terr Atmos Ocean Sci* 2013;**24**:695–707.

Yakimov MM, Golyshin PN, Lang S *et al*. *Alcanivorax borkumensis* gen. nov., sp. nov., a new, hydrocarbon-degrading and surfactant-producing marine bacterium. *Int J Syst Evol Microbiol* 1998;**48**:339–48.